Journal of Energetic Materials
Publication details, including instructions for authors and subscription information:
http://www.informaworld.com/smpp/title~content=t713770432

Thermal initiation of high explosives by electron beam heating

A. Stolovy[a]; A. I. Namenson[a]; J. B. Aviles Jr.[a]; E. C. Jones Jr.[a]; J. M. Kidd[a]
[a] Naval Research Laboratory, Washington, D.C.

To cite this Article Stolovy, A. , Namenson, A. I. , Aviles Jr., J. B. , Jones Jr., E. C. and Kidd, J. M.(1987) 'Thermal initiation of high explosives by electron beam heating', Journal of Energetic Materials, 5: 3, 181 — 238
To link to this Article: DOI: 10.1080/07370658708012352
URL: http://dx.doi.org/10.1080/07370658708012352

THERMAL INITIATION OF HIGH EXPLOSIVES BY ELECTRON BEAM HEATING

A. Stolovy, A.I. Namenson, J.B. Aviles, Jr.,
E.C. Jones, Jr. and J.M. Kidd
Naval Research Laboratory, Washington D.C. 20375

A 40-MeV electron beam has been used to uniformly heat confined samples of high explosives until explosion occurs. From observations of temperature vs time, values were obtained for the thermal initiation thresholds (deposited energy per gram until explosion) and explosion temperatures. These are good indicators of thermal explosion sensitivity. In many cases, the specific heat or the latent heat of fusion were obtained. Data were obtained on the following materials: HMX, PBX-9404, RDX, HBX-1, Comp. A-3, PBXW-109, TATB, TNT, DNP, DIPAM, NDAC, TNB and TNBA. Thermal threshold values vary from 57 cal/gm to 168 cal/gm for these materials. There is some indication that these results are correlated with data from impact sensitivity tests. Radiation-induced decomposition is shown to be very small.

Journal of Energetic Materials vol. 5, 181-238 (1987)

Published in 1987 by Dowden, Brodman & Devine, Inc.

INTRODUCTION

The behavior of energetic materials subjected to thermal stimulus has usually been studied by slow heating techniques such as differential scanning calorimetry, differential thermal analysis, thermogravimetric analysis and pyrolysis on unconfined samples. These have yielded much valuable information on the thermal properties and kinetics of the chemical reactions[1]. Isothermal cook-off experiments have also been done, sometimes with spherical geometry[2] to simplify the analysis. Time-to-explosion measurements with slab or spherical geometry[3-5] have yielded valuable information. Another technique is the thermal step test[6,7], in which a pulse of electric current heats a capillary tube containing a small sample of explosive, and the induction time to explosion is measured as a function of the temperature.

The technique we have developed[8-10] makes it possible to uniformly heat confined samples of energetic materials at a variety of heating rates, and to observe the temperature and gas pressure as a function of time until explosion occurs, usually in a few seconds. This is done by irradiating the confined high explosive (HE) samples with a high energy (40 MeV) electron beam from the NRL Linac. The beam is very penetrating, depositing only a small portion of its energy in the HE sample. Beam profile measurements show that, within 10 percent, energy is deposited in the HE

sample uniformly, so that thermal gradients are very small, and the results are independent of the size and shape of the sample. Thus, the thermal behavior of HE materials can be obtained from relatively small samples. These experiments yield information on thermal initiation thresholds (deposited energy per gram, or dose required to initiate a runaway chemical reaction), explosion temperatures and physical or crystalline phase transitions. The thermal initiation threshold is obtained directly from the product of the beam heating rate and the irradiation time until explosion.

There do not seem to be any previous systematic measurements of thermal initiation thresholds or explosion temperatures for confined HE samples. Phung[11] has done some calculations of critical doses and initiation temperatures based upon a hot spot model, and also performed some experiments with a 1-MeV electron beam striking small unconfined samples. For RDX and HMX, his experiments gave only a lower limit of 40 cal/g for the "critical dose", and the calculations yielded values of about 38 cal/g, which are much lower than our experimental results with confined samples. These early results cannot be compared to our measurements, which were performed under quite different conditions. The experiments that are closest to those reported here are time-to-explosion experiments in which confined samples are placed in

fixed temperature baths.[3-5] A critical bath temperature is defined as the temperature below which no explosion occurs. This critical temperature is dependent on the size and shape of the sample, and is obtained from experiments which often involve long heating times ($> 10^3$ sec) during which much of the HE has decomposed. Critical temperature values are tabulated in several compilations.[1,12] However, these data cannot be related to the data reported here, in which the thermal energy is deposited almost uniformly and rapidly, so that the samples initiate before appreciable decomposition has occurred. This point will be decussed in detail in the discussion of results section.

This report is intended to be a survey of the work we have done in recent years, so that the data can be available at this time. An analysis of some of the points associated with this technique is given in the discussion section. A more detailed analysis will be given in a subsequent report.

EXPERIMENTAL PROCEDURES

The following HE materials have been examined in this investigation: HMX,PBX-9404, RDX, HBX-1, Comp. A-3, PBXW-109, TATB, TNT, DNP, DIPAM, NDAC, TNB and TNBA. Some of the HE samples were fabricated at the Naval Surface Weapons Center in the form of a pair of pressed powder disks, each 0.718 cm

diameter by 0.470 cm thick, with a total weight of 0.5 to 0.7 g. Other samples were pressed in our laboratory using a die with a diameter of 0.732 cm. The samples were confined within a stainless steel cell as shown in Fig. 1. The junction of a small (0.0025 cm diameter) iron-constantan thermocouple is pressed between the two HE disks which are surrounded by ceramic cloth insulating material. Indium solder is used to seal in the reaction product gases. In some experiments, a pressure transducer was attached to obtain data on pyrolytic gas pressure as a function of time. The rear (downstream) window is 0.08 cm thick Al alloy, and is designed to blow out at pressures exceeding 2.8×10^7 Pa (4000 psi). The front (upstream) window is 0.32 cm thick Al alloy. All experiments were performed in air, with the electron beam emerging from a water-cooled exit window. The confinement cells are usually placed about 12 cm from the Linac exit window to ensure a uniform beam profile across the HE sample. Heating rates can be changed by varying this distance, or by changing the pulse repetition rate. The Linac exit window is protected from explosion debris by a 0.32 cm thick Al plate, or by bending the beam away from the exit window with a magnet. A computer is used for data acquisition and for producing plots of temperature or pressure vs time. In some experiments, data were also obtained with chart recorders.

The pulsed beam parameters usually used in these experiments were as follows: 40 MeV average energy, 1 μs pulse width, 320 mA peak current, and 360 pulses/s repetition rate. At a distance of 12 cm from the Linac exit window, heating rates were typically about 10 cal g^{-1} s^{-1}, corresponding to about $40^{o}C/s$. Heating rates more than an order of magnitude greater are possible at a position close to the Linac exit window, but at the expense of the uniformity of irradiation.

The beam profile was measured at the sample position (12 cm from the Linac exit window) by two methods. In the first method, we exposed 5 X 5 arrays of calcium fluoride thermoluminescent detector squares (each with 0.318 cm sides) to 5 beam pulses, and read them on a calibrated TLD reader. These results showed that the beam was uniform within 10 percent over the HE target area. In the second method, radiachromic films (which darken upon exposure) were placed at the sample position and read out at a densitometer. A plot of horizontal and vertical scans through an exposed film is shown in Figure 2. This indicates that over the area of the HE sample, the beam is uniform to within 8 percent.

The HE heating rates are obtained in two ways: from the HE itself and from an Al calorimeter. The heating rate from the HE data is obtained from the slope of the temperature vs.

time curve at the midpoint of the initial inactive region (before exothermic reactions or phase changes occur). The product of this slope and the heat capacity at this temperature is the observed beam heating rate. This is a little less than the true beam heating rate because of small conductive cooling losses, but the observed heating rate is the actual rate at which the HE sample is absorbing energy. The thermal initiation threshold is then the product of this observed heating rate and the beam irradiation time until explosion, If a latent heat process such as melting or a crystalline phase transformation occurs before explosion, the time to explosion will increase (because of the additional beam heating time required to affect the phase change), thus increasing the thermal threshold by an amount equal to the latent heat of the phase change. The calorimeter is an Al alloy disk, 0.718 cm in diameter by 0.318 cm thick with an attached thermocouple junction, placed close to and upstream from the HE sample, as indicated in Fig. 1. Data from this calorimeter is particularly useful when the specific heat of the HE is not known.

A steel collimator, 2.54 cm thick is placed upstream from the confinement cell to reduce activation of the cell by scattered electrons. It is important to insure that the cell is electrically grounded; otherwise charge build-up from the beam produces a very noisy thermocouple output. The low

melting point materials TNT, NDAC and TNB presented a special problem in that the molten HE would be absorbed by the soft insulating material, thus leaving the beam area. For these materials, machined insulators made from lava rock ceramic were used instead of soft insulation. For most of the materials we have examined, melting or crystalline phase changes are observed before explosion. In many cases, explosion occurs during or immediately after melting, so that the explosion temperature is approximately the same as the melting point.

EXPERIMENTAL DATA

In the following, we do not give chemical names or formulations of mixtures for the more well-known HE materials; these can be found in compilations of HE properties, such as Ref. 1. We give such information only for a few less well-known materials.

1. HMX

This material is known to exhibit four crystalline phases[13]. As the material is heated, a crystalline phase transformation from the β to the δ phase occurs at about 185°C, and appears as a plateau on a temperature vs time plot, as shown in Fig. 2. The abscissa is also given in dose units at the top of the figure. The origin of a second plateau which appears just before explosion in most of the tests is not clear. It is probably associated with the RDX

impurity which is always present in military grade HMX, but we did not have chemically pure HMX available to perform tests to confirm this. A combination of exothermic reactions in HMX and melting of non-uniformly distributed RDX impurity could produce this behavior, and the observed fluctuations in explosion temperature. It should be noted that it is important to study standard HE materials which contain impurities which affect their thermal behavior. The results of nine experiments on pressed powder HMX pellets with no binders are summarized in Table 1. Threshold values were obtained from the HE and from the Al calorimeter, as previously explained. The average threshold values obtained by these two methods are in good agreement, but there is a systematic difference between the HE and calorimeter data. This will be discussed later. The uncertainties shown are standard deviations of the mean; i.e., the standard deviation divided by the square root of the number of experiments. This is correct if we assume that a fixed mean value can be assigned to each explosive. Blanks in the table indicate portions of the data which were poor due to a noisy thermocouple signal.

TABLE 1

Thermal Initiation of HMX Samples.

Beam Heating Rate (cal g^{-1} s^{-1})		Time Until Explosion (s)	Thermal Threshold (cal/g)		Explosion Temperature (°C)
HE	Calor.		HE	Calor.	
4.39	4.83	13.48	59.1	65.1	215
3.88	4.18	15.80	61.3	66.0	---
3.97	4.10	14.32	56.8	58.7	245
4.99	5.32	12.90	64.3	68.7	245
5.01	5.35	12.15	60.9	65.0	255
6.53	7.00	10.28	67.1	72.0	---
6.30	----	9.87	62.2	----	235
9.88	8.88	7.05	69.6	62.6	260
3.00	2.76	19.11	57.3	58.6	+30
		Averages:	62.1 ± 1.4	64.6 ± 1.6	241 ± 6

2. PBX-9404

This often-used material, which is 94 percent HMX, would be expected to have thermal initiation properties similar to that of HMX. An example of data taken with this material is shown in Fig. 3. Explosion occurs suddenly and violently. Indeed, in two of the eight experiments performed, a transition to high-order detonation seemed to occur, blowing out the 0.318 cm thick Al entrance window as well as the 0.08 cm exit window. The data for the eight experiments are

TABLE 2

Thermal Initiation of PBX-9404.

Beam Heating Rate (cal g^{-1} s^{-1})		Time Until Explosion (s)	Thermal Threshold (cal/g)		Explosion Temperature (°C)
HE	Calor.		HE	Calor.	
9.65	8.33	6.24	60.2	52.0	271
11.28	9.68	5.91	66.7	57.2	276
11.25	10.76	5.81	65.3	62.5	278
10.51	9.59	6.00	63.1	57.5	269
11.14	10.54	5.95	66.3	62.7	293
8.15	8.12	7.50	61.1	60.9	277
7.62	6.90	8.30	63.2	57.3	282
9.77	9.72	6.44	62.9	62.6	290
		Averages:	63.6 ± 0.8	59.1 ± 1.3	280 ± 5

listed in Table 2, showing good consistency. The threshold values obtained from the HE and calorimeter differ by more than one standard deviation. The threshold obtained from the HE is in excellent agreement with the value obtained with pure HMX, but results from the calorimeter data are quite different. The explosion temperature for PBX-9404 is considerably higher than that for HMX, probably because this material does not have the RDX impurity present in our HMX samples.

3. RDX

This is another basic nitramine explosive often used in

combination with other materials. The data for RDX, as given in Fig. 4, shows evidence of exothermic activity before the melting point plateau at about 200°C, and then a rapid runaway reaction to explosion from the molten material. Although the explosions are quite energetic, there is no evidence for a transition to high-order detonation, as observed in HMX-based explosives. In Table 3, we list the data from nine experiments. Agreement between the two threshold averages is good. The observed explosion temperature is simply the melting point.

TABLE 3

RDX Thermal Initiation Data.

Beam Heating Rate (cal g^{-1} s^{-1})		Time Until Explosion (s)	Thermal Threshold (cal/g)		Explosion Temperature (°C)
HE	Calor.		HE	Calor.	
10.26	9.93	7.29	74.8	72.4	207
8.98	9.96	7.06	63.4	70.3	203
10.26	9.93	6.80	69.8	67.6	200
9.90	7.62	7.43	73.6	56.6	201
9.59	9.24	6.79	65.1	62.8	203
11.84	11.14	5.13	60.8	57.2	203
14.04	14.47	4.58	64.3	66.3	196
14.80	12.97	4.52	66.9	58.6	192
6.62	6.96	9.30	61.5	64.7	196
		Averages:	66.7 ± 1.7	64.1 ± 1.9	200 ± 2

4. HBX-1

This is a mixture of RDX, TNT, aluminum powder and wax. An example of a beam heating curve for this material is shown in Fig. 5. The flattening of the curve near 80°C and 200°C are due to melting of the TNT and RDX components, respectively. A detailed look at the exothermic region is shown in Fig. 6, where the interval between points is 1.39 ms (two data points between beam pulses). The exotherm is seen to start from the melt plateau, and then the curve flattens out near 660°C, where the Al powder melts. A runaway exotherm to explosion occurs after all the aluminum has melted. Also shown are data obtained with a pressure transducer[9] on pyrolytic gas pressure, which shows no structure as it rises monotonically to rupture. The initiation data for ten experiments are listed in Table 4. The HE and calorimeter data are in reasonable agreement.

The threshold and explosion temperature are both slightly higher than those for RDX, possibly due to the influence of the TNT, but RDX seems to dominate the thermal initiation of this material.

TABLE 4

Thermal Initiation of HBX-1 Samples.

Beam Heating Rate (cal g^{-1} s^{-1})		Time Until Explosion (s)	Thermal Threshold (cal/g)		Explosion Temperature (°C)
HE	Calor.		HE	Calor.	
20.12	--	3.34	67.2	--	196
10.30	9.76	6.88	70.9	67.1	205
9.18	8.05	8.36	76.7	67.3	220
9.08	7.80	7.70	69.9	60.1	200
9.23	8.95	7.13	65.8	63.8	225
6.84	5.66	10.50	71.8	59.4	230
6.76	6.95	10.15	68.6	70.6	215
9.18	9.21	7.83	71.9	72.1	230
8.87	9.36	7.98	70.8	74.7	220
9.86	9.20	7.48	73.7	68.8	210
		Averages:	70.7 $\pm$ 1.0	67.1 $\pm$ 1.7	215 $\pm$ 4

5. Comp. A-3

This material is 91 percent RDX and 9 percent wax binder. A previous investigation[14] had indicated that the addition of small amounts ($\leq$ 1 percent) of saligenin will desensitize this material, as demonstrated by impact tests. Therefore, we performed a series of experiments using electron beam uniform heating to see if the thermal initiation threshold is affected by the addition of saligenin[15]. The

TABLE 5

Thermal Initiation of Comp. A-3. Small Amounts of Saligenin were added as indicated.

Beam Heating Rate ($cal\ g^{-1}\ s^{-1}$)	Time Until Explosion (s)		Thermal Threshold (cal/g)		Explosion Temperature (^{o}C)	
Percent Saligenin	HE	Calor.		HE	Calor.	
0	4.23	4.90	14.37	60.8	70.4	191
0	10.79	11.28	5.27	56.9	59.5	191
0.1	14.97	13.93	4.16	62.1	58.0	192
0.1	5.44	5.49	12.35	67.2	67.8	208
0.1	5.16	6.56	8.77	45.2	57.6	180
0.2	9.59	12.80	4.10	39.3	52.5	170
0 2	5.56	5.21	8.50	47.3	44.3	192
0.4	8.24	8.52	6.52	53.7	55.6	191
0.4	6.38	4.84	11.71	74.8	56.7	240
0.6	4.92	5.72	9.56	46.9	54.5	190
0.6	10.83	8.90	7.16	77.5	63.8	225
0.6	4.39	6.25	10.22	44.9	63.9	178
0.6	5.94	7.90	7.92	47.1	62.6	176
0.8	15.30	13.20	4.35	66.5	57.3	238
0.8	12.53	11.35	5.49	68.8	62.3	211
1.0	14.57	11.27	4.81	70.1	54.2	250
1.0	5.49	7.30	9.80	53.8	71.5	175
1.0	4.98	6.63	9.25	46.1	61.3	175
	Averages:			57.2 ± 2.8	59.7 ± 1.6	199 ± 6

RDX content was always 91 percent, while the saligenin content was varied between 0 percent and 1 percent. The results are listed in Table 5. An examination of these results shows no dependence of thermal initiation characteristics on saligenin content. We therefore obtained average values for the entire set of experiments as shown. There is a considerable amount of fluctuation in these data. The average threshold is a little lower than that for pure RDX but the difference is not statistically significant. A typical heating curve is shown in Fig. 7; it looks very similar to the behavior of RDX.

6. PBXW-109

This is another RDX-based explosive. An example of a beam heating curve is shown in Fig. 8. The melting of RDX is seen as the plateau-like region near 200°C, but the plateau is not completely flat. The beam heating and reaction continue beyond the melt region to explosion at a considerably higher temperature than observed for RDX or Comp. A-3. The tabulated results of nine tests are listed in Table 6. The specific heat for RDX was used in calculating the HE beam heating rate and threshold. The threshold from the HE data is in agreement with the result for RDX. The calorimeter data yield a considerably higher value.

TABLE 6

Thermal Initiation of PBXW-109.

Beam Heating Rate (cal g^{-1} s^{-1})		Time Until Explosion (s)	Thermal Threshold (cal/g)		Explosion Temperature (°C)
HE	Calor.		HE	Calor.	
8.11	7.92	8.40	68.1	66.5	265
8.15	7.81	8.01	65.3	62.6	255
9.00	11.24	7.13	64.2	80.1	240
8.91	10.86	7.23	64.4	78.5	251
9.01	10.46	7.19	64.8	75.2	245
9.68	9.18	7.12	69.0	65.3	250
11.21	11.11	6.06	67.9	67.3	248
10.94	11.73	6.29	68.8	73.8	248
10.08	11.46	6.49	65.5	74.4	245
		Averages:	66.4 ± 0.7	71.5 ± 2.1	250 ± 4

7. TATB

This HE is known to be less sensitive to thermal or shock initiation than the nitramines. We obtained values of 145 ± 4 cal/g and 409 ± 6 °C for the thermal initiation threshold and explosion temperature, respectively. We have previously reported[9] extensively on this material, so it will not be discussed here.

8. TNT

This material was experimentally difficult to work with,

because its melting point is much lower than the explosion temperature. In order to hold the liquid TNT in the beam, we replaced the soft insulating material shown in Fig. 1 by lava rock ceramic insulators. The thermocouple signal from the liquid HE was often very noisy, possibly due to gas bubbles and erratic thermal contact. Some of the samples did not explode until extraordinary doses were deposited (>340 cal/g); some did not explode at all. Only 5 out of 14 experiments yielded reasonably consistent results, with relatively quiet thermocouple signals. These are tabulated in Table 7. An example of the data is shown in Fig. 9. The melting plateau at about 80°C is clearly seen, but explosion does not occur until much later. The average thermal threshold is greater than any of the other materials we studied. A portion of this threshold is due to the latent heat of fusion. Assuming that the beam is the only heating source during the melting process (no exothermic chemical reactions occur at 80° C), we can obtain values of the latent heat of fusion from the product of the beam heating rate and the duration of the plateau; we obtain an average value of 24 ± 2 cal $g^{-1}{}^{o}C^{-1}$.

The explosion temperatures are quite high and exhibit a considerable amount of fluctuation.

TABLE 7

Thermal Initiation of TNT.

Beam Heating Rate (cal g^{-1} s^{-1})		Time Until Explosion (s)	Thermal Threshold (cal/g)		Explosion Temperature (^{o}C)
HE	Calor.		HE	Calor.	
5.30	5.45	33.8	179.2	184.0	295
7.90	7.27	21.8	171.9	158.1	300
32.90	--	5.24	172.2	--	370
19.97	14.59	9.34	186.5	136.3	375
12.21	13.49	10.57	129.0	142.6	310
		Averages:	168 ± 12	155 ± 11	330 ± 18

9. DNP (Dinitropiperazine)

The thermal behavior of DNP is shown in Fig. 10. It exhibits an unusually long melting plateau at about 215°C, and explodes at slightly above the melting point. The duration of this plateau varies considerably between tests, resulting in fluctuations in the thermal threshold values. The results are tabulated in Table 8. The explosion temperature was not obtained for the first run because of a noisy thermocouple signal. Since the specific heat of this material is unknown, heating rates and thresholds were obtained from the calorimeter data alone. These data can then be used together with the slope of the HE curve (below the melting plateau) to obtain an average value of 0.34 ± 0.04 cal g^{-1} $^{o}C^{-1}$ for the specific heat between room temperature and 200°C.

TABLE 8

Thermal Initiation Data for DNP. Beam Heating Rates and Thresholds are from Calorimeter Data.

Heating Rate (cal g^{-1} s^{-1})	Time Until Explosion (s)	Thermal Threshold (cal/g)	Explosion Temperature (°C)
8.79	13.97	122.6	---
9.30	13.85	128.8	213
9.63	17.15	165.2	225
9.12	17.00	155.0	240
9.07	14.77	133.9	225
10.26	14.14	145.1	220
7.22	13.77	99.5	214
9.25	11.96	110.6	222
7.00	12.27	85.9	215
8.91	11.86	105.7	224
6.73	16.56	111.4	220
Averages:		124 ± 7	222 ± 3

10. DIPAM (Dipicramide)

Nine confined samples of this HE were exposed to a deflected beam which, unfortunately, was poorly aligned in some cases, resulting in low heating rates. Four runs were considered to be unreliable, and discarded. The data for the good runs are given in Table 9.

TABLE 9

Thermal Initiation Data for DIPAM.

Beam Heating Rate (cal g^{-1} s^{-1})		Time Until Explosion (s)	Thermal Threshold (cal/g)	
HE	Calor.		HE	Calor.
8.69	8.83	14.15	122.9	124.9
11.49	10.79	10.62	122.1	114.6
11.95	13.76	8.15	97.4	112.2
9.84	10.45	13.32	131.1	139.2
11.77	10.33	13.40	157.7	138.5
		Averages:	126 ± 10	126 ± 6

There is a considerable amount of fluctuation between these results, which is due to large variations in the duration of the melting plateau at about 300°C. The agreement between the HE and calorimeter average values is fortuitous. A typical data curve is given in Fig. 11. The explosion temperature is the melting point in all cases.

11. NDAC (Nitraminodiacetonitrile)

Since this HE has a low melting point, we used ceramic insulators to contain the liquid. A heating curve is given in Fig. 12, showing a long melting plateau at about 90°C, and explosion at about 250°C. The data are given in Table 10. Since the HE specific heat is unknown, we list heating

rates and thresholds obtained from the calorimeter only. Some of the runs were done with rather low heating rates, probably due to beam misalignment. Because cooling losses are a considerable fraction of the beam heating rate for these runs, we obtained average calorimeter heating rates from the midpoint of these curves. For two of the runs, explosion temperatures could not be obtained because of noisy thermocouple signals, probably due to bubbles in the melted HE. By comparing the initial slopes of the HE and calorimeter curves, we can obtain values of the specific heat for the region between $20^{o}C$ and $90^{o}C$; we thus obtain an average specific heat of 0.30 ± 0.04 cal g^{-1} $^{o}C^{-1}$. Since melting occurs well below the onset of exothermic reactions, we can also obtain values for the latent heat of fusion from the product of the heating rate and the duration of the plateau. This leads to an average value of the latent heat of 31 ± 3 cal/g.

TABLE 10

Thermal Initiation Data for NDAC. Beam Heating Rates and Thresholds are from Calorimeter Data.

Beam Heating Rate (cal g^{-1} s^{-1})	Time Until Explosion (s)	Thermal Threshold (cal/g)	Explosion Temperature (^{o}C)
4.37	18.11	79.2	215
16.12	5.70	91.8	225
9.94	12.05	119.7	---
11.55	11.39	131.5	---
4.19	26.6	111.5	230
6.86	16.72	114.8	265
7.26	16.30	118.4	270
5.02	25.5	128.0	290
	Averages:	112 $\pm$ 6	249 $\pm$ 12

12. TNB (Trinitrobenzene)

This material behaved quite erratically. Although ten samples were irradiated, five of them would not explode at all, and instrumental problems developed in two others. Thus, we obtained data on only three experiments; the results are listed in Table 11 for the calorimeter data only, since

TABLE 11

Thermal Initiation Data for TNB. Beam Heating Rates and Thresholds are from Calorimeter Data.

Beam Heating Rate (cal g^{-1} s^{-1})	Time Until Explosion (s)	Thermal Threshold (cal/g)	Explosion Temperature (^{o}C)
12.57	10.75	135.2	350
11.08	13.52	149.8	310
10.27	13.58	139.5	260
	Averages:	142 ± 4	307 ± 26

the HE specific heat is not known. The heating rates are average values, taken at the midpoint of the irradiation time. The threshold and explosion temperature are quite large. Ceramic insulators were used to confine the melted HE. Fig. 13 shows a melting plateau at about 110^{o}C, and explosion at about 310^{o}C. By comparing the initial slope of the HE and calorimeter data, we obtain an average value for the specific heat of 0.32 ± 0.04 cal g^{-1} $^{o}C^{-1}$, for the region between 20^{o}C and 100^{o}C. From the plateau lengths, we obtain an average value of the latent heat of fusion of 24 ± 4 cal/g.

13. TNBA (Trinitrobutyric Acid)

This material has a very low melting point, so ceramic insulators were used to keep the liquid HE in the beam. A typical heating curve is shown in Fig. 14, exhibiting a melting plateau at about 60°C, and explosion at about 235°C. The results of seven experiments are given in Table 12. The

TABLE 12

Thermal Initiation Data for TNBA. Beam Heating Rates and Thresholds are from Calorimeter Data.

Beam Heating Rate (cal g^{-1} s^{-1})	Time Until Explosion (s)	Thermal Threshold (cal/g)	Explosion Temperature (°C)
7.48	15.35	114.8	235
8.13	11.04	89.8	235
8.32	11.62	96.7	235
10.56	8.37	88.4	228
9.23	9.76	90.1	240
10.04	10.18	102.2	225
8.57	10.49	89.9	237
	Averages:	96.0 ± 3.7	234 ± 2

heating rates and thermal thresholds were obtained from the calorimeter data only, since the HE specific heat is not known. Again, we can obtain values of the specific heat from the ratio of the initial calorimeter heating rate to the initial slope of the HE curve. This yields an average value of 0.28 ± 0.03 cal g^{-1} $^{o}C^{-1}$, for the interval $20^{o}C$ to $60^{o}C$. We also obtain values of the latent heat of fusion from the plateau lengths; the average value is 16 ± 3 cal/g.

DISCUSSION OF RESULTS

1. Thermal initiation characteristics

A summary of the thermal initiation thresholds and explosion temperatures for the 13 HE materials we have examined is given in Table 13. In many cases, thermal threshold values obtained from the HE and calorimeter data differ by several standard deviations. When the specific heat[1] of the HE was known as a function of temperature, we have listed the result obtained directly from the HE as the best value, but with an uncertainty reflecting the spread in results obtained from the HE and the calorimeter. When the specific heat was not previously known, we have listed thresholds obtained from the calorimeter, with errors which include uncertainty in a geometrical correction factor (since the Al calorimeter is not quite in the same position as the HE). Thus, all the errors quoted in Table 13 are larger than the statistical standard deviation of the mean values given in the previous section.

TABLE 13

Thermal Initiation Characteristics of High Explosives from Electron Beam Heating Experiments.

Explosive	Thermal Threshold (cal/g)	Explosion Temperature (°C)
HMX	63 ± 4	240 ± 6
PBX-9404	64 ± 3	280 ± 5
RDX	67 ± 5	200 ± 4
HBX-1	71 ± 5	215 ± 5
Comp.A-3	57 ± 5	199 ± 8
PBXW-109	66 ± 5	250 ± 4
TATB	145 ± 4	409 ± 6
TNT	168 ± 12	330 ± 18
DNP	124 ± 7	222 ± 4
DIPAM	126 ± 10	304 ± 5
NDAC	112 ± 10	249 ± 15
TNB	142 ± 15	307 ± 30
TNBA	96 ± 5	234 ± 4

The PBX-9404 initiation parameters are very similar to that of pure HMX. Similarly, the RDX-based materials (HBX-1, Comp. A-3 and PBXW-109) have initiation parameters that are within about 20 percent of those for RDX. It should be noted that although HBX-1 also contains TNT, its thermal initiation is dominated by the more sensitive RDX component. TATB has a

threshold which is about twice that of the HMX or RDX-based materials. The threshold for TNT is still higher. There is much interest in the last five materials listed although they are not in common usage; they have fairly high thresholds, so they should be thermally stable. The order of explosion temperatures does not necessarily follow the order of thermal thresholds, because the latter is affected by latent heat processes (usually melting). Thus, the threshold for TNT is greater than that for TATB, although its explosion temperature is lower.

As a by-product of these experiments, we often obtain information on other thermal properties of these explosives. These are listed in Table 14. We obtained the latent heat of

TABLE 14

Thermal Properties of High Explosives from Electron Beam Heating Experiments.

Explosive	Melting Point (°C)	Latent Heat of Fusion (cal/g)	Specific Heat (cal g^{-1} $°C^{-1}$)	Temperature Range (°C)
TNT	80	24 ± 2	--	--
DNP	215	--	0.34 ± 0.04	20 — 200
NDAC	90	31 ± 3	0.30 ± 0.04	20 — 90
TNB	115	24 ± 4	0.32 ± 0.04	20 — 100
TNBA	60	16 ± 3	0.28 ± 0.03	20 — 60

fusion only for those cases where the melting point is well below the explosion temperature, so that we can be reasonably sure that exothermic reactions have not yet begun, and the beam is the only heat source during the melting process. Specific heat values were obtained only for those materials for which it was not previously measured[1]. These are average values over the temperature range indicated in the last column.

Considerable fluctuation is observed between individual threshold measurements on the same HE material, and also between the HE and calorimeter data. It is not clear if these fluctuations are due to experimental errors, variations between the samples, small differences in experimental conditions or the statistical nature of energetic material behavior. To obtain good average values, it is necesssary to perform many nearly identical experimental tests. Our best results were obtained for materials on which 8 or more tests were done.

2. Comparison with impact tests

It is interesting to compare our thermal initiation parameters with impact sensitivity tests, such as drop hammer, gap and Susan tests. This is difficult because impact test results are often strongly dependent upon density, grain size, binder, humidity and the test apparatus[16]. Petersen[17] has made a critical evaluation of these tests, has

normalized them to a common hazard index and ranked them according to an average index for all tests. We have looked for correlations between our results and these impact tests. Since the probability distributions are not known for any of these data, it is best to use a distribution-free test such as the correlation by ranks[18] or the disarray test [18]. Although either of these tests would be appropriate, we have used the disarray test because it runs faster on a computer, greatly facilitating Monte Carlo analysis of the data. It is also more accurate when the number of data points is small. We have assumed that a negative correlation is not physically meaningful, so we have calculated the one-sided significance of correlation.[18] Thus, a comparison of our thermal initiation threshold and explosion temperature values with impact tests yield the significance of correlation values given in Table 15, for the 10 cases in which there are overlapping data.

TABLE 15

Significance of Correlation Between Thermal Initiation and Impact Tests in Percent, for 10 Explosives.

	Average, Drop Hammer Tests	Average, Gap Tests	Average, All Impact Tests
Thermal Threshold	95	85	92
Explosion Temperature	91	92	95

These numbers indicate that a correlation exists between our thermal initiation data and the impact tests, but it is not strong. In fact, there is less than a 0.5 percent chance that the data are totally correlated. However, the correlation improves to significant levels ($>$ 99 percent) if we use the impact data for cast TNT, rather than pressed. Apparently, cast powder samples are much less sensitive to impact initiation than pressed samples are, but this is not true for our thermal initiation tests, which are sensitive only to the chemistry of the material, not its mechanical properties. Monte Carlo checks on these data indicate that our assigned uncertainties are reasonable; i.e., the significance levels do not change much when the results are varied within the quoted uncertainties. The correlation between thermal and impact tests is not surprising, because in impact tests, the kinetic energy is converted to heat.

3. Thermal decomposition

In this section, we present some general features of the thermal initiation process which are applicable to these experiments (thermal gradients assumed negligible) based upon the simplest model available: a first order reaction in which the rate constant has an Arrhenius temperature dependence. The basic equations are:

$$dN/dt = -ZN \exp[-E/RT] \qquad (1)$$

$$C_v \, dT/dt = \dot{q} + QZN \exp[-E/RT] \, , \qquad (2)$$

in which:

N = fraction of original material

Z = frequency factor (s^{-1})

E = activation energy (cal/mole)

Q = heat of reaction (cal/g)

$\dot{q}$ = beam heating rate (cal g^{-1} s^{-1})

C_v = heat capacity at constant volume (cal g^{-1} $^oC^{-1}$)

As the system approaches initiation, the chemical energy release term in Eq. (2) makes a transition from a value which is small compared to $\dot{q}$ to a value which greatly exceeds it. It is natural to introduce a temperature T_e at which the chemical term becomes equal to $\dot{q}$:

$$\dot{q} = QZN_e \exp[-E/RT_e] \, . \qquad (3)$$

We identify T_e with the explosion temperatures found experimentally and listed in Table 13.

To obtain an estimate of the decomposition fraction up to the explosion temperature, we divide Eq. (1) by Eq. (2), integrate, and note that the result is dominated by the upper temperature limit T_e. For the decomposition fraction at

T_e, we obtain:

$$(1-N_e) \lesssim C_v T_e^2 \ln 2 / Q(E/R). \quad (4)$$

If we consider TNT, and use the values Q = 300 cal/g, E = 34.4 Kcal/mole and C_v = 0.33 cal g^{-1} $^oC^{-1}$ from Ref.1, and our value T_e = 330°C (603°K), we obtain $(1- N_e) \leq 0.0163$. For HMX, $(1- N_e) \leq 0.0040$. In general, the model predicts very little decomposition up to the explosion threshold. Experimental evidence for this can be seen by examining the exothermic region in HBX-1 shown in Figure 7. Evidence for gaseous decomposition products appears as a pressure rise only after the initiation threshold. Further evidence comes from recent studies by Sharma[19] of electron-beam irradiated HE samples; he found very little decomposition, even for doses near threshold.

The temperature rise at threshold due to the exothermic reaction can similarly be shown to be small. It is given by:

$$\Delta T_e = (1-N_e)Q/C_v \lesssim T_e^2 \ln 2 /(E/R). \quad (5)$$

For TNT and HMX, ΔT_e is less than 14.7°C and 6.7°C, respectively. Therefore, almost all of the decomposition and self-heating occurs in the exothermic reaction beyond threshold.

This simple model does not include effects due to phase changes or impurities (these could be modeled). It serves

only to show how useful information can be obtained by this method, and to estimate the parameters of the reaction.

4. Radiation-induced decomposition

When a high energy (many MeV) beam electron strikes a molecule, an atomic electron is usually ejected, leaving the ionized molecule highly excited. The ejected electron collides with other molecules in a cascading process until the energy is distributed over many excited ionized molecules with an average excitation energy I.

The molecules can deexcite in several ways, one of which is unimolecular decomposition, where the rate of decomposition is proportional to the energy deposition rate:

$$dN/dt = -\alpha \dot{q} N \ , \tag{6}$$

where α is the fractional decomposition per unit deposited energy:

$$\alpha = (\Delta N/N)/\Delta q \ , \tag{7}$$

where $\Delta q = \dot{q}\, \Delta t$, and ΔN and Δq are small. Integration of Eq. (6) yields

$$N = \exp[-\alpha q], \quad \text{where} \quad q = \int_0^t \dot{q}\, dt \tag{8}$$

is the energy deposited in a time t.

The quantity $N\, \Delta q$ is the total energy deposited per unit

mass in the undecomposed molecules by a beam electron. Initially this energy is confined to a small number of molecules, ΔN. If all these molecules decompose, $N\Delta q = I\Delta N$. Comparing this to Eq. (7), we see that $\alpha^{-1} = I$. This implies that we could use average values of I to obtain estimates of radiative decomposition. For a typical HE molecule, $I \approx 80$ eV, which is a large excitation energy (due to predominantly inner shell ionization) compared to the energy to break a molecular bond. Thus radiative decomposition is energetically possible.

In order to experimentally study radiative decomposition, we performed a series of experiments in which unconfined 0.12 g samples of TNT were irradiated to varying total doses. The irradiations were done very differently from the other experiments in this report, since our objective was to avoid thermal decomposition. The combination of a low pulse rate (15/s), an Al conducting holder and a blower fan prevented any appreciable temperature rise. The irradiated samples were then chemically analyzed by thin layer chromatography[20] to determine the fraction decomposed as a function of deposited energy. The results are shown in Fig. 16. This semi-logarithmic plot shows that the results are reasonably consistent with the exponential form given in Eq. (8). From the least-squares fitted slope, $\alpha^{-1} = 3.70 \times 10^9$ rads. Expressed in more useful units, $\alpha^{-1} = 8850$ cal/g or

α^{-1} = 87.1 MeV/molecule. We can now estimate the amount of radiative decomposition at explosion from Eq. (8), using q_e = 168 cal/g for TNT:

$$N_e = \exp[-168/8850] = 0.98 \ . \qquad (9)$$

Thus the non-thermal radiative effect accounts for only about 2 percent of the decomposition in the explosion.

The average excitation of a molecule is a weighted average over the atoms in the molecule. For the atoms H, C, N and O, I = 17.6, 77.3, 76.8 and 98.5 (in eV) respectively.[21] For TNT, this average is I = 69.1 eV, which is reasonably close to the experimental value α^{-1} = 87.1 eV. Thus, it seems reasonable to use average values of I to obtain estimates of radiative decomposition at threshold for other HE material using Eq. (8). The results for TATB, HMX and RDX are about 2, 1 and 1 percent, respectively; i.e., it is very small in all cases.

The radiative decomposition of a molecule is accompanied by energy absorption (bond breaking) or energy release (exothermic decomposition). Let us designate the average energy change per unit mass by Q_r, which can be either positive of negative. Assuming no thermal decomposition, the rate equation is:

$$C_v \, dT/dt = \dot{q} - Q_r \, dN/dt = \dot{q}[1 + \alpha Q_r] \qquad (10)$$

from Eq. (6), with $N \approx 1$. We do not know the magnitude of Q_r; if it is comparable to the heat of reaction, then $\alpha Q_r \approx 0.03$. In principle, this energy change would show up as a difference between thresholds obtained from the HE and the inert calorimeter. However, the effect is probably too small to see. The data show many differences between HE and calorimeter average threshold results which are not consistent. This suggests a systematic error which varies from run to run that has not yet been uncovered. However, the difference is not large, indicating that αQ_r must be small.

In summary, we have shown that under the conditions studied in this paper, radiative effects produce only a very small amount of decomposition products, which would be unlikely to have any observable effect on the thermal properties of the HE. The beam energy is deposited almost entirely thermally; i.e., it increases the internal energy of the system, producing the observed temperature rise. Corroborative evidence comes from a study of molecular fragmentation in sub-initiated TATB[22], which showed that the decomposition products from electron beam and normal heating are very similar, while impact and UV produce different products. These considerations give us confidence that rapid uniform electron beam heating is a valid technique for studying the thermal and initiation properties of energetic materials.

5. Effect of beam heating rate

We have previously[8] indicated that the explosion temperature and thermal threshold may be weakly (logarithmically) dependent on the beam heating rate, as can be seen by solving Eq. (3) for T_e. Holtkamp[23] has examined our data to search for this. In our experiments, the thermal thresholds are calculated from the product of the beam heating rates and times to explosion, so that any experimental errors in the beam heating rates will be propagated into the thresholds, producing non-physical calculational correlations. To avoid this problem, we look for anti-correlations of the times to explosion with the thresholds, because the times to explosion are measured with good precision (errors $<$ 1 percent), so there are essentially no errors propagated to the threshold values. Again, it is necessary to apply distribution free statistics, so we have used the disarray test[18] (for the same reasons mentioned in the section on comparison with impact tests). The results of these calculations are given in Table 16.

In most cases, the fluctuations in results (even for experiments done with approximately the same heating rates) precludes the possibility of observing a significant correlation. In the case of HMX, a real anti-correlation appears. On the basis of these data, we cannot draw any

conclusions about a general dependence of thresholds on heating rates.

TABLE 16

Correlation of Times to Explosion with Thermal Initiation Thresholds, Using the Disarray Test

Explosive	Number of Experiments	Corr. or Anti	Significance of Correlation
HMX	9	Anti	0.98
PBX-9404	8	Anti	0.82
RDX	9	Corr	0.23
HBX-1	10	Corr	0.62
Comp. A-3	18	Anti	0.27
PBXW-109	9	Anti	0.86
TATB	7	Corr	0.86
TNT	5	---	0.00
DNP	11	Corr	0.78
DIPAM	5	Corr	0.77
NDAC	8	Anti	0.45
TNB	3	---	0.00
TNBA	7	Corr	0.76

SUMMARY

We have shown that a high energy electron beam can be used to heat confined HE samples uniformly and rapidly to obtain thermal initiation data. Almost all of the thermal

decomposition occurs after threshold. Radiation-induced decomposition was shown to be very small. Thermal thresholds and explosion temperatures were shown to be correlated with impact test results. An anti-correlation between thermal thresholds and beam time to explosion was found for HMX, but not for the other HE materials.

ACKNOWLEDGMENTS

We are grateful to J.W. Forbes and H.G. Adolph at NSWC for supplying us with the HE samples examined in this paper. We thank W.A. Fraser who performed most of the data acquisition work. Discussions with C.S. Coffey at NSWC and D. Holtkamp at LANL were very useful. We appreciate the efforts of K.D. Gage and R.M. Farr who operate the Linac and assisted with the experiments.

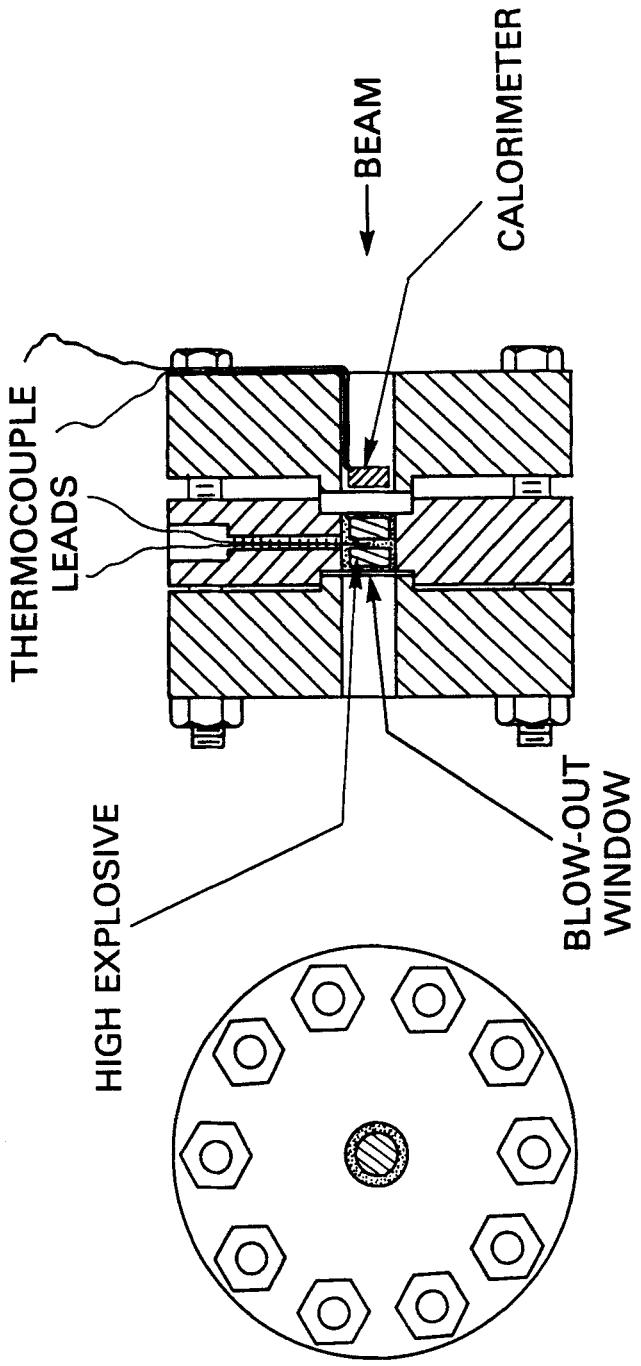

FIGURE 1
Stainless steel confinement cell for HE. The outside diameter of the cell is 7.0 cm.

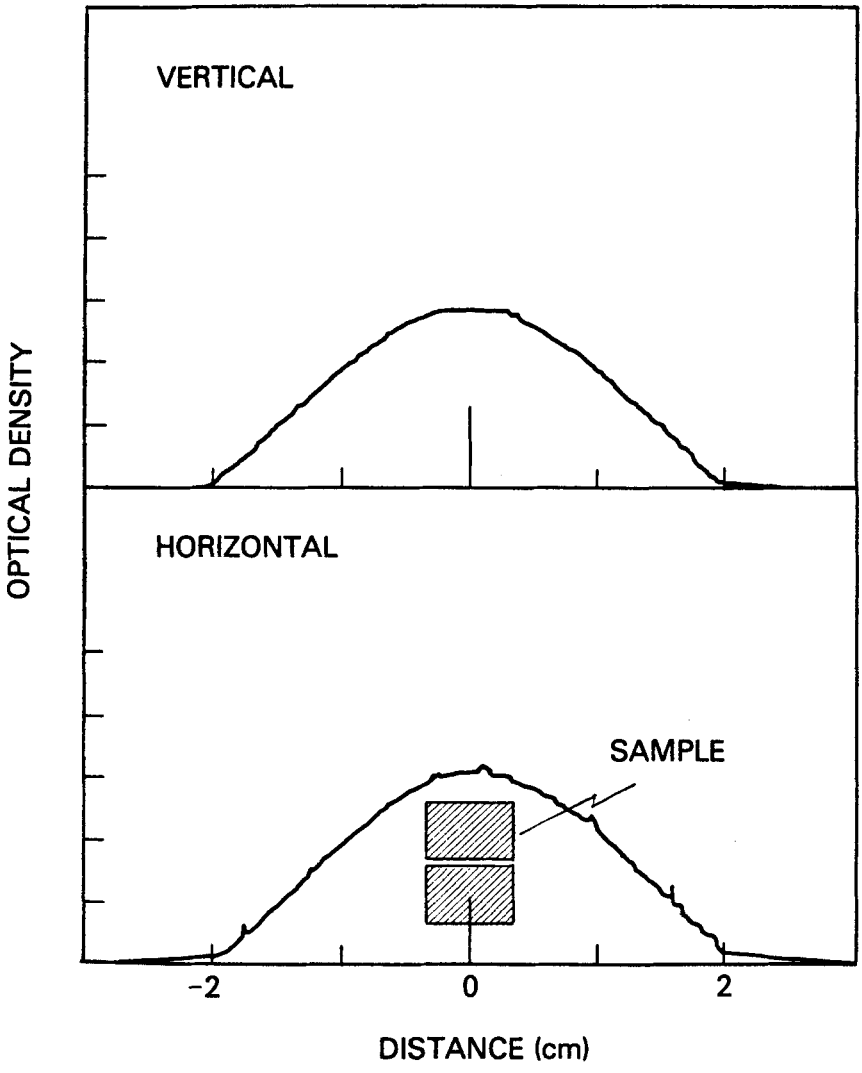

FIGURE 2
Beam profile densitometer plot from radiachromic film exposure to 1000 pulses.

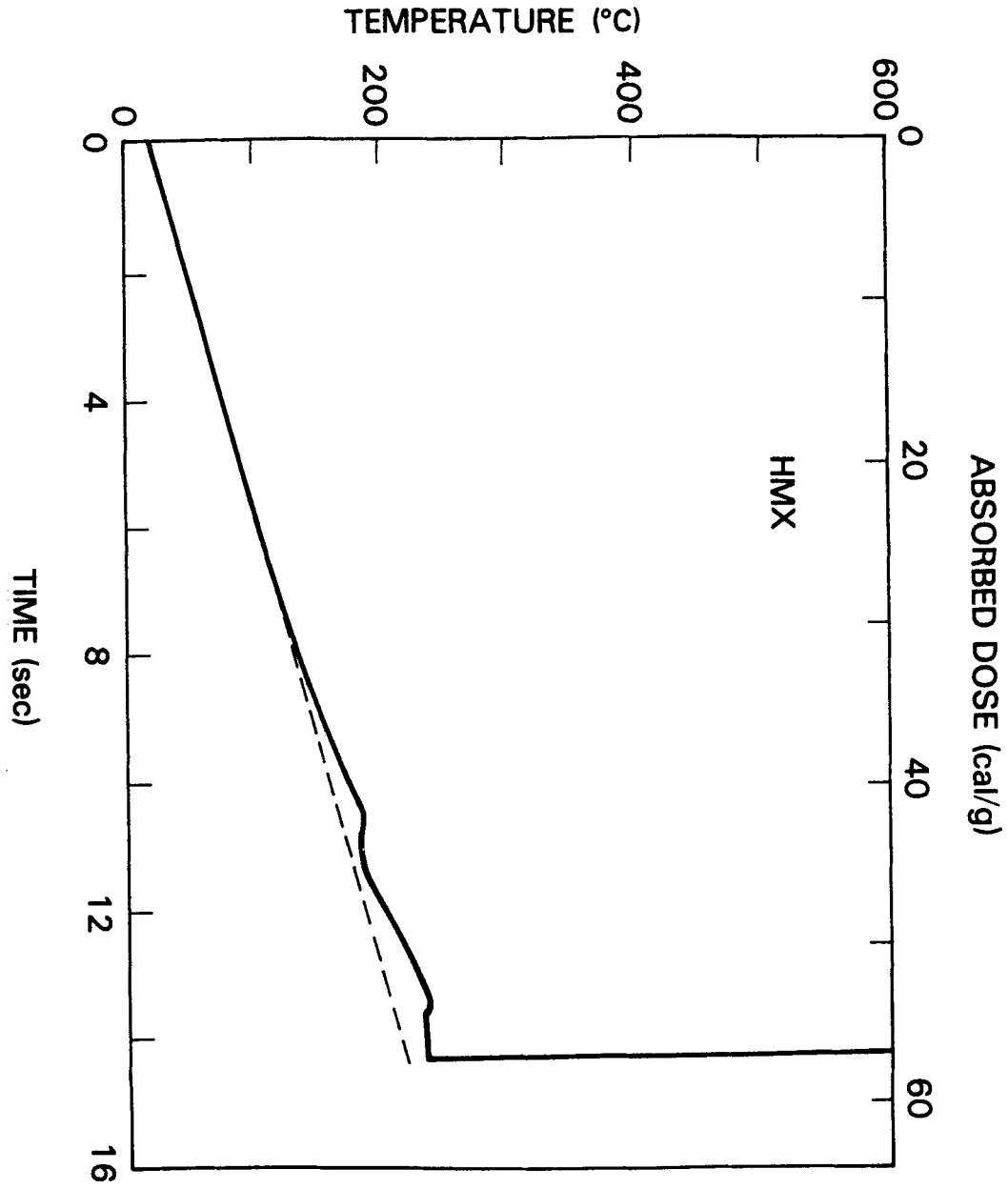

FIGURE 3
Thermal behavior of confined HMX (no binder) heated by electron beam. The dashed line represents the beam heating.

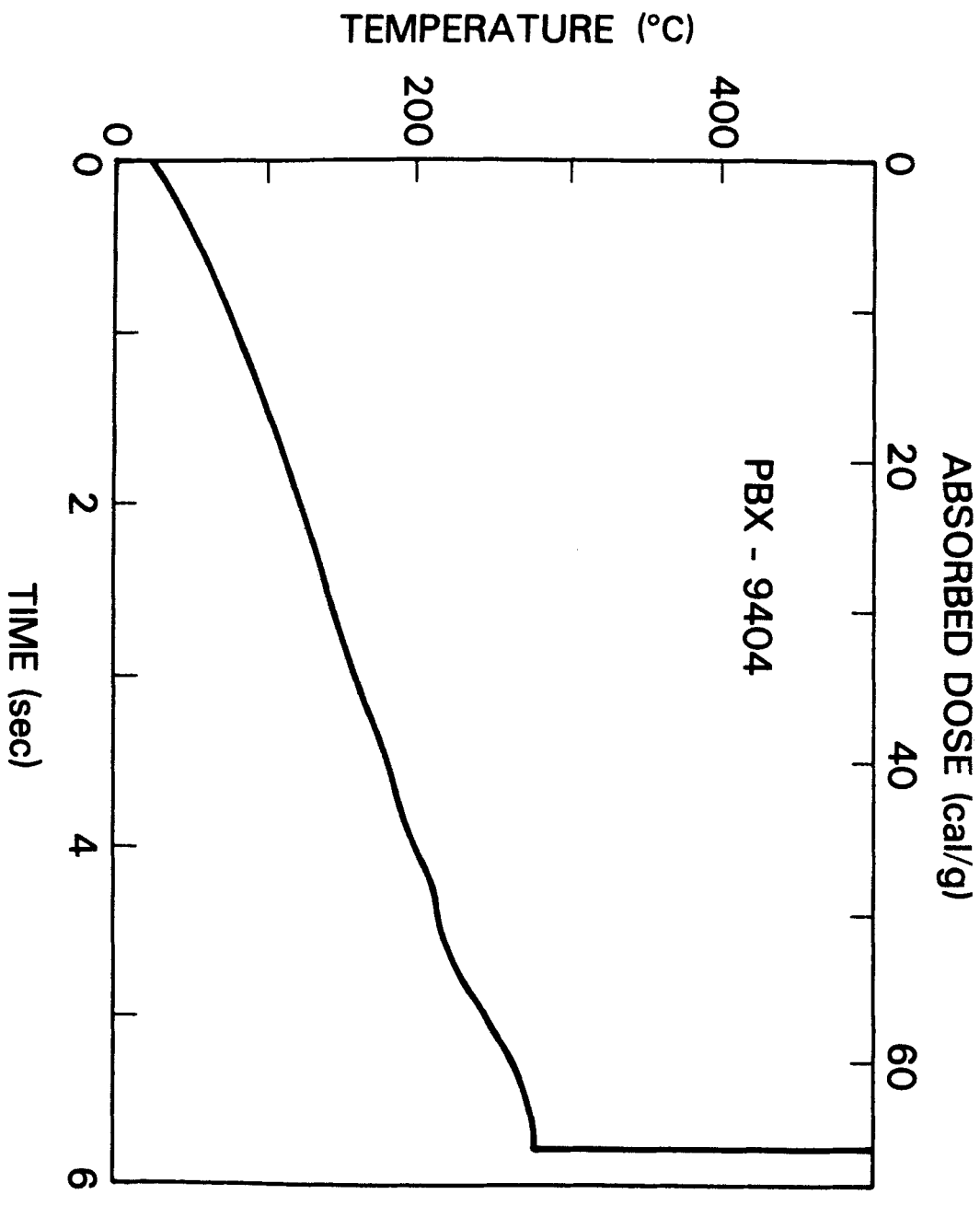

FIGURE 4
Thermal behavior of confined PBX-9404 under beam heating.

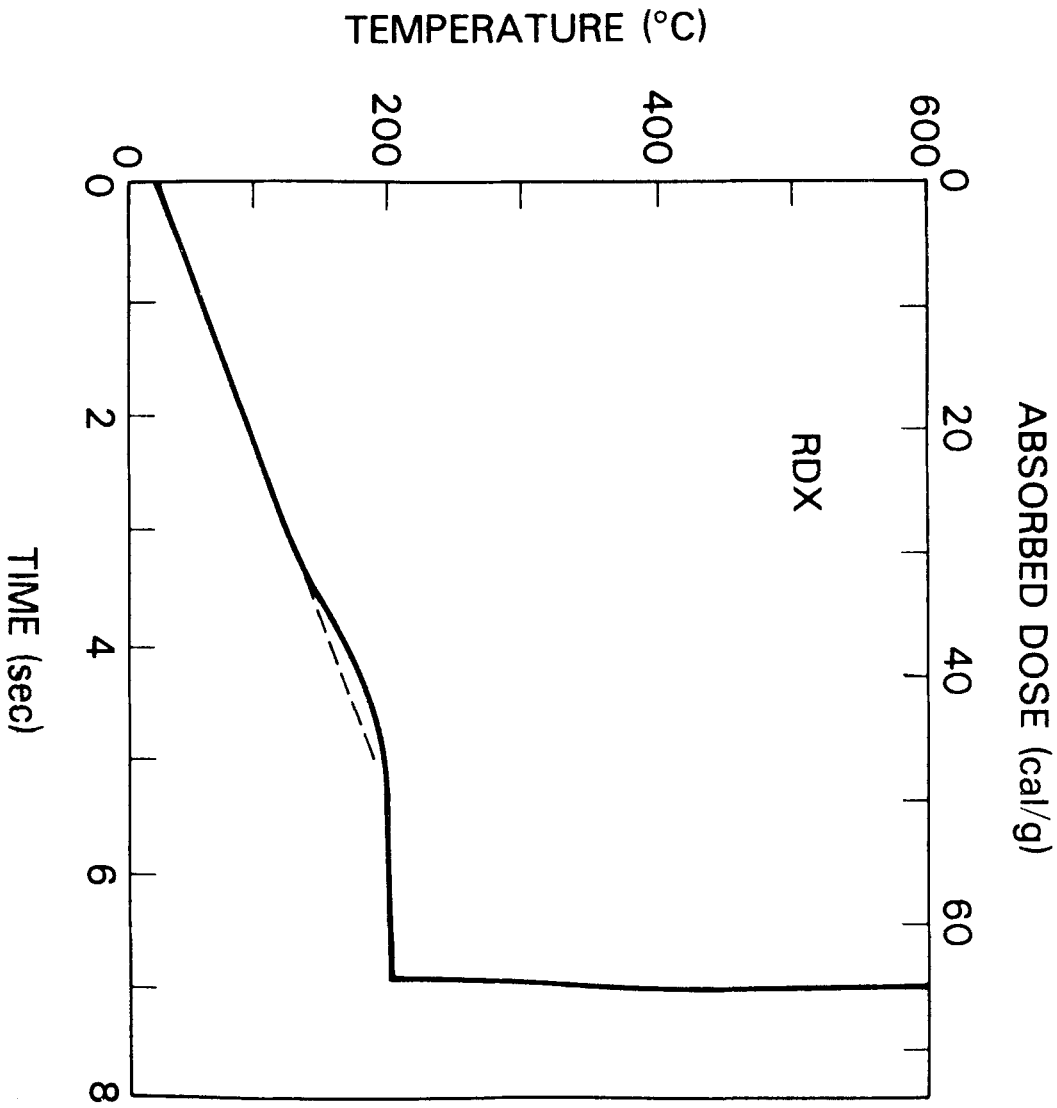

FIGURE 5
Thermal behavior of confined RDX (5 percent zinc stearate binder) heated by beam. The dashed line represents the beam heating.

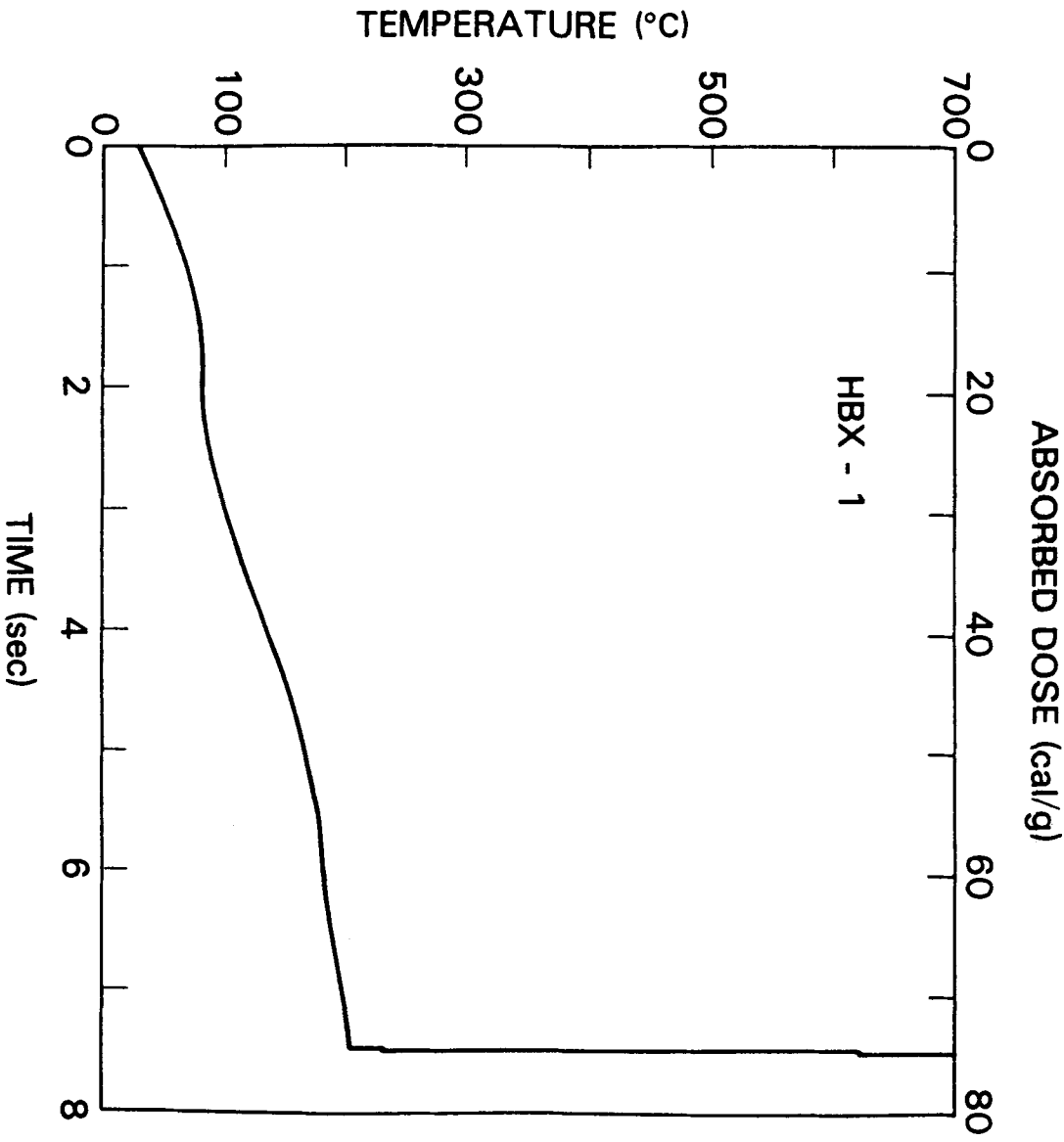

FIGURE 6
Thermal behavior of confined HBX-1 under beam heating.

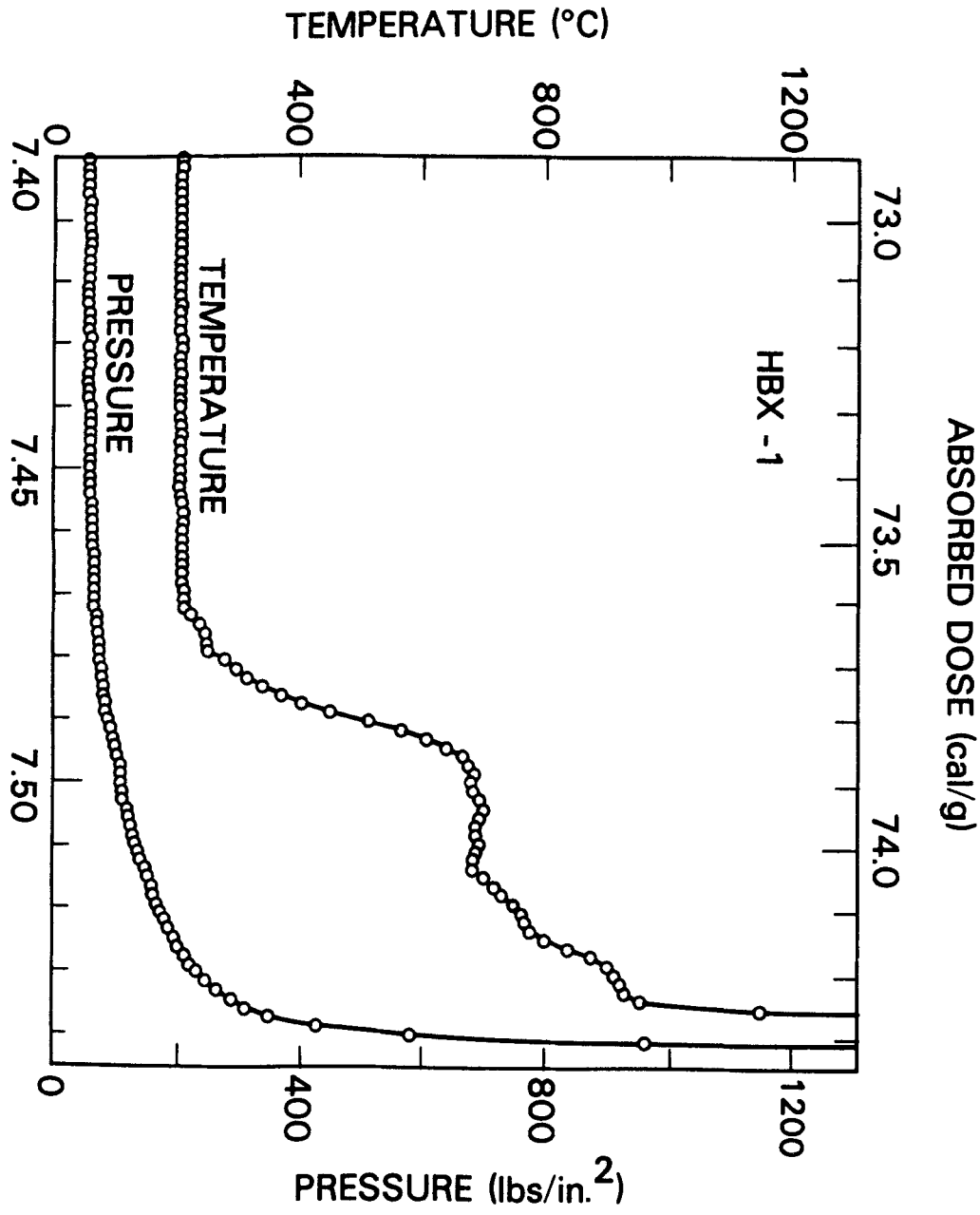

FIGURE 7
Exothermic region of thermal initiation of confined HBX-1.

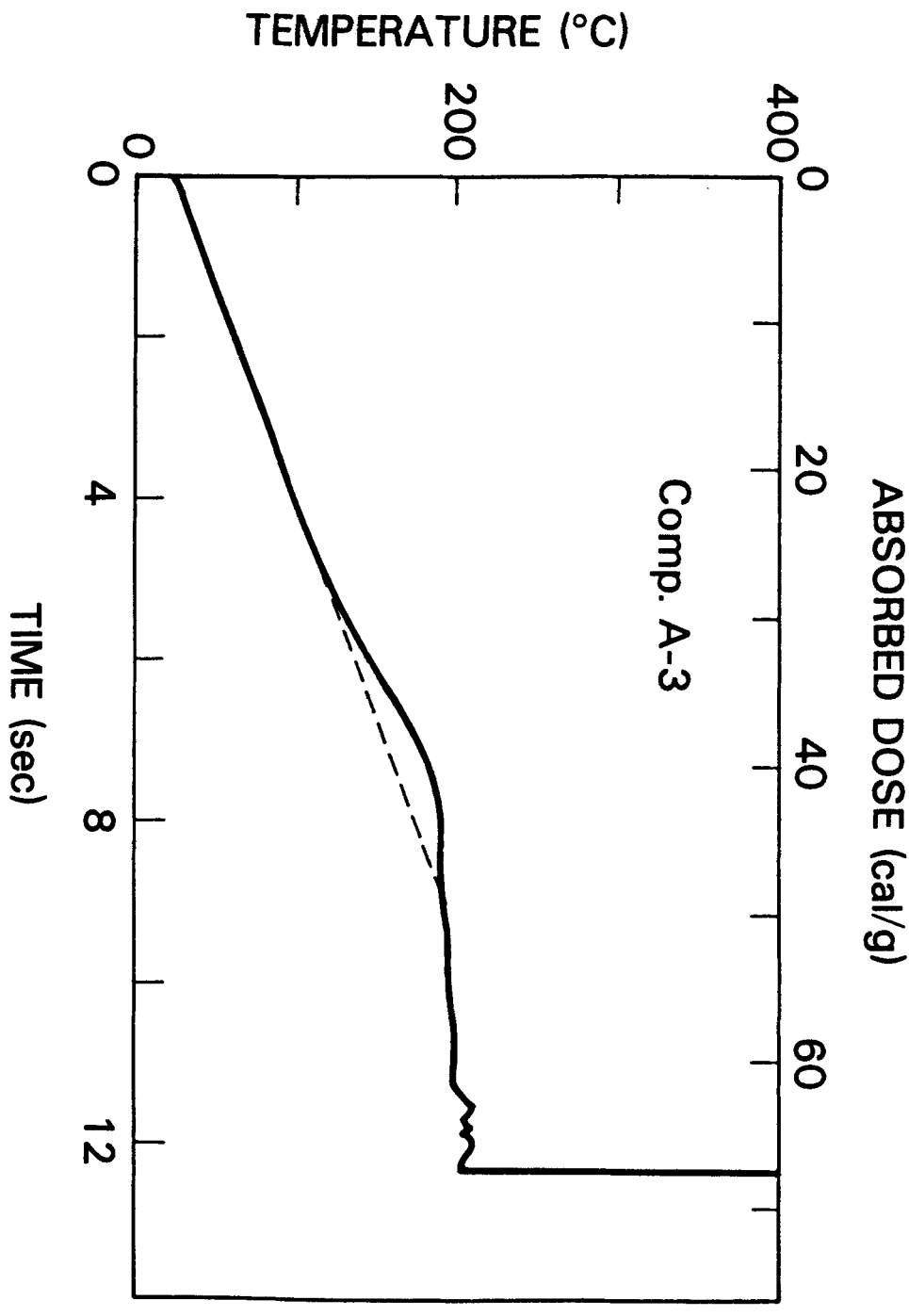

FIGURE 8
Thermal behavior of confined Composition A-3. The dashed line represents beam heating.

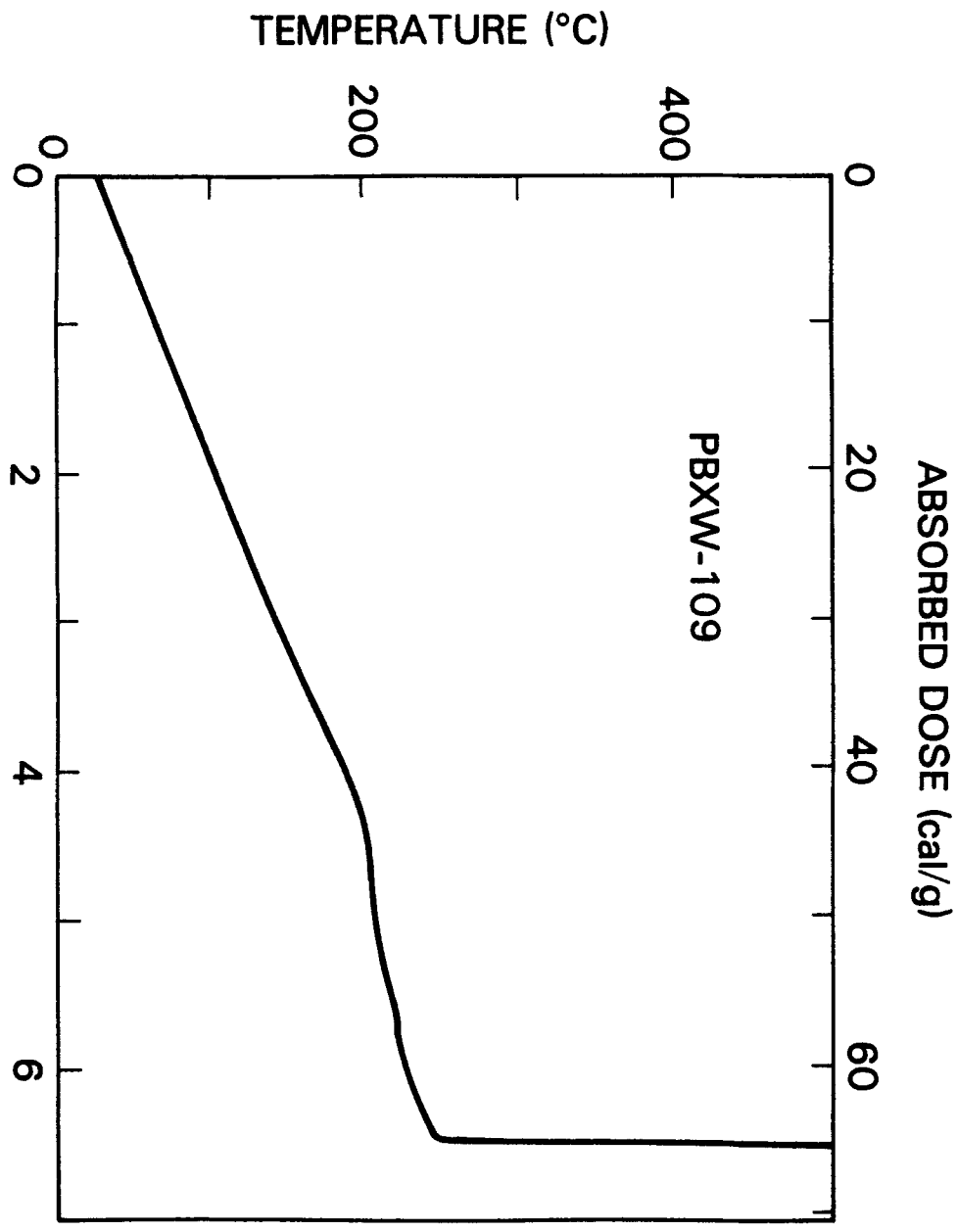

FIGURE 9
Thermal behavior of confined PBXW-109 heated by beam.

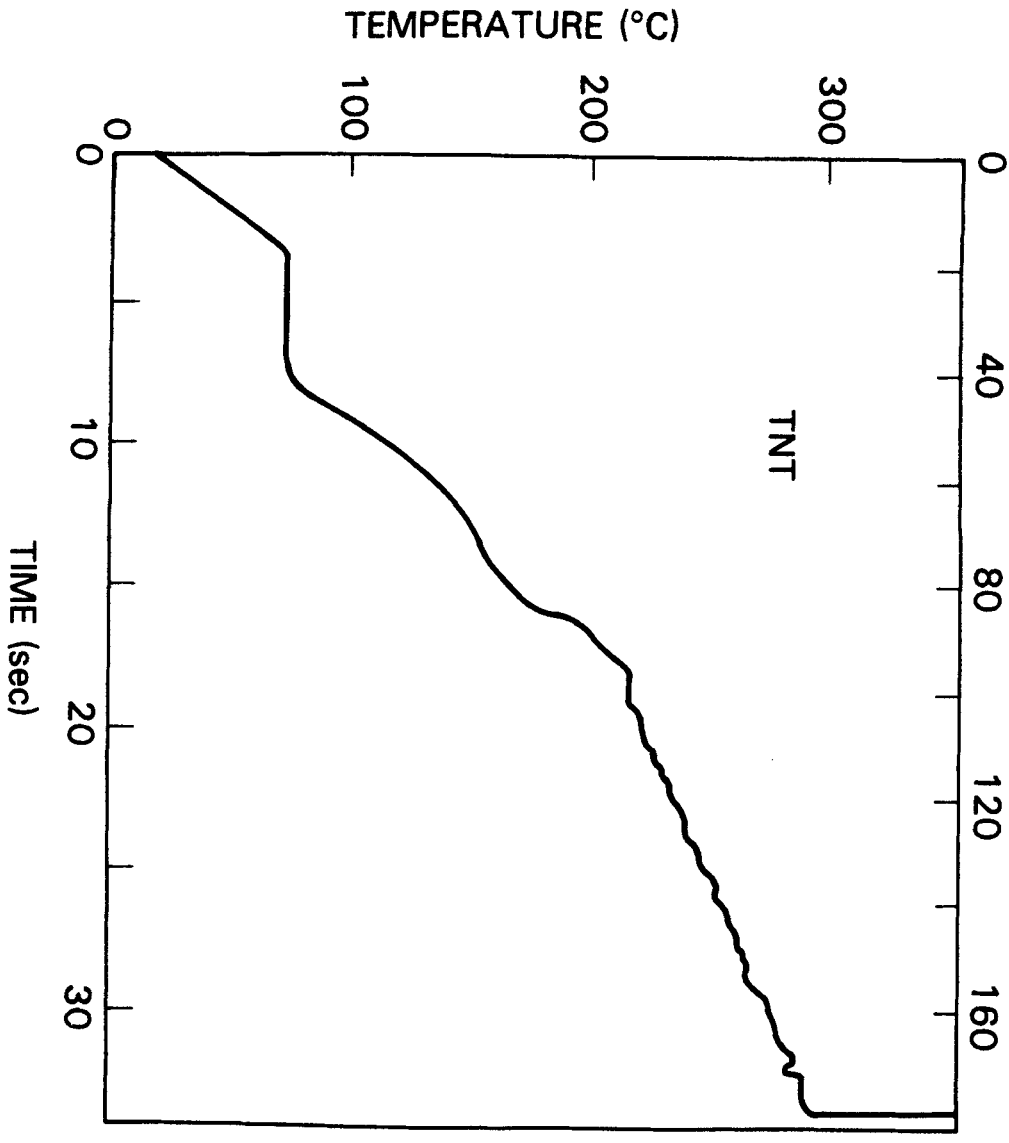

FIGURE 10
Thermal behavior of confined TNT under beam heating. The TNT is liquid above the melting plateau.

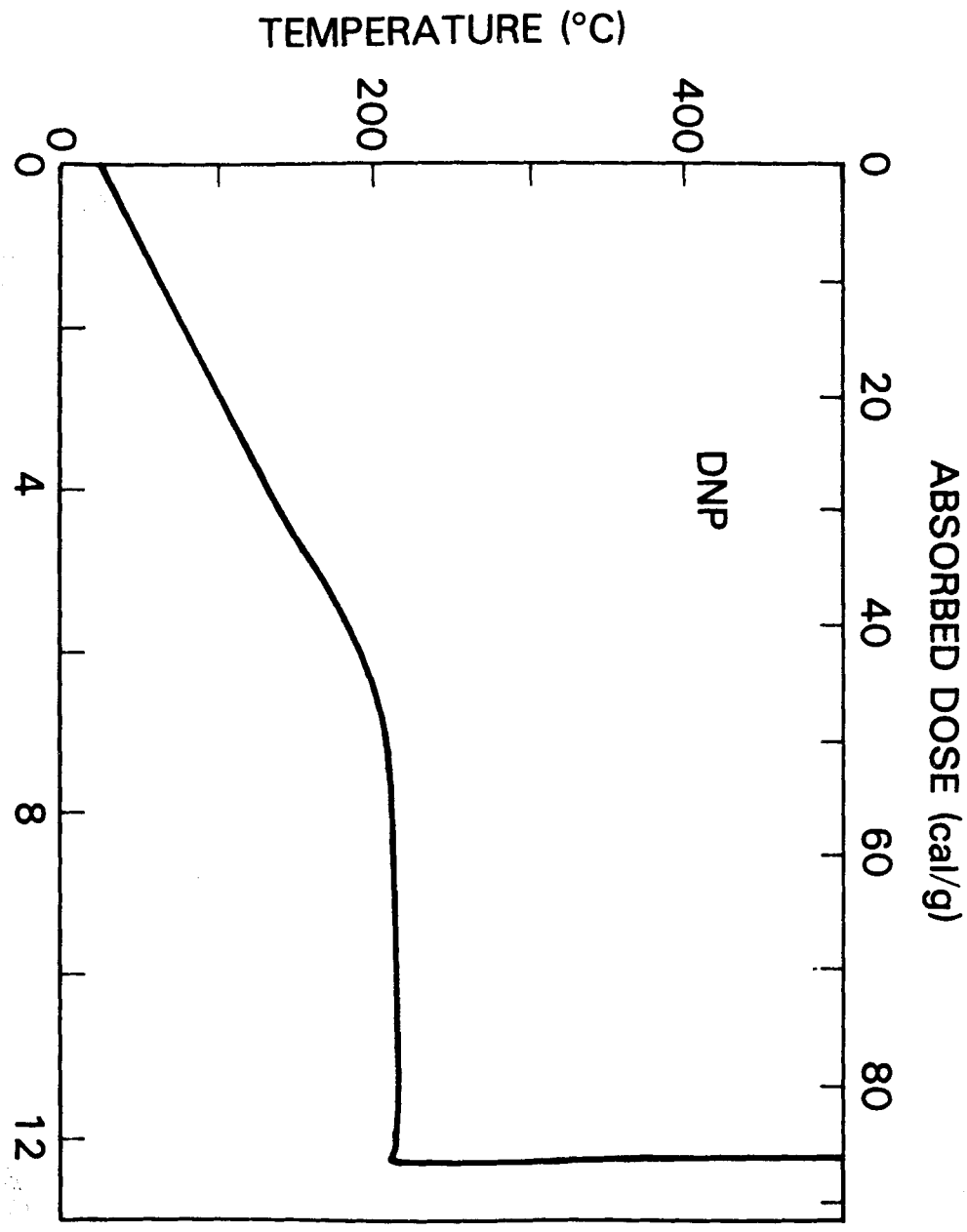

FIGURE 11
Thermal behavior of confined DNP under beam heating.

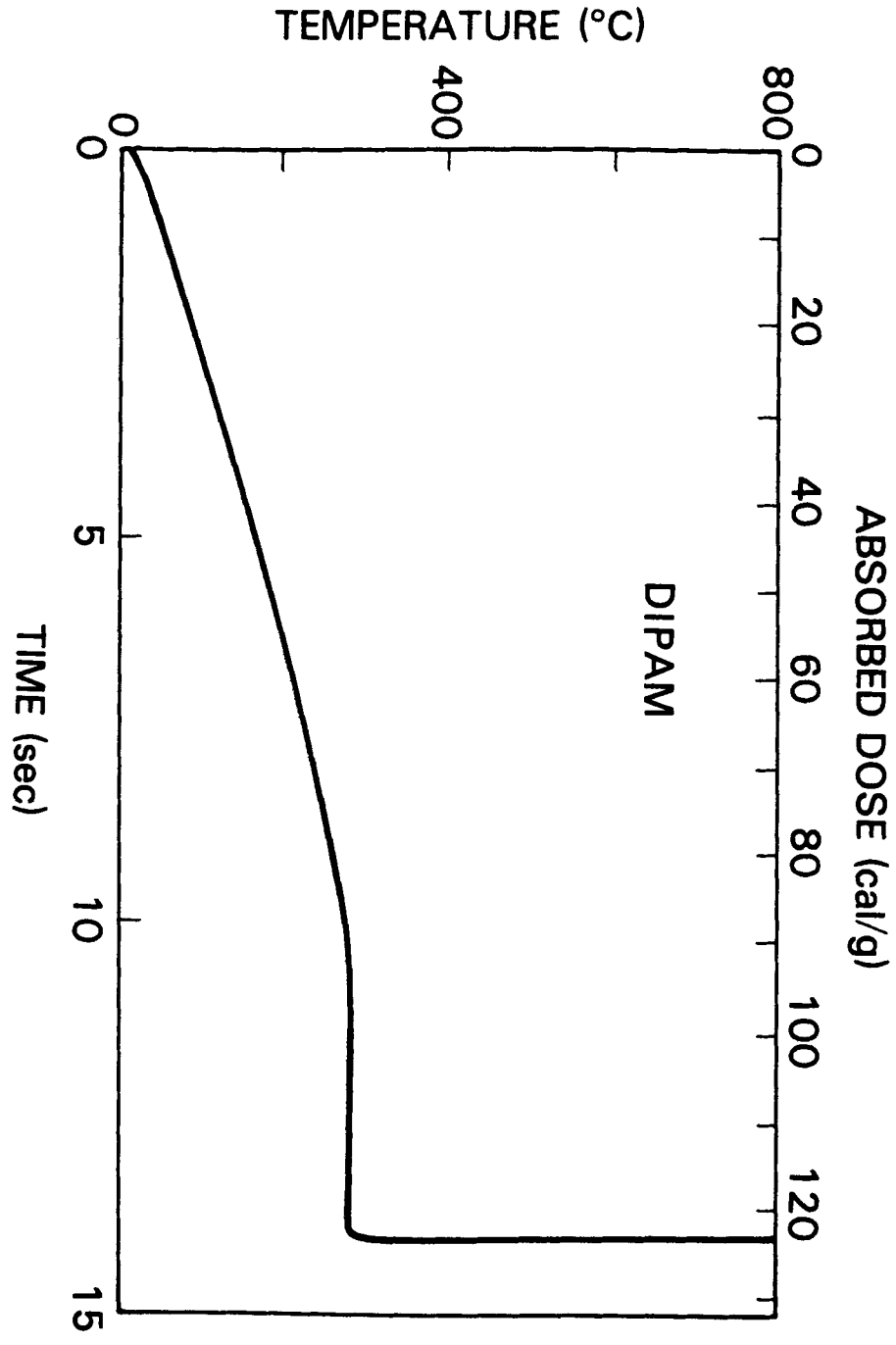

FIGURE 12
Thermal behavior of confined DIPAM heated by beam.

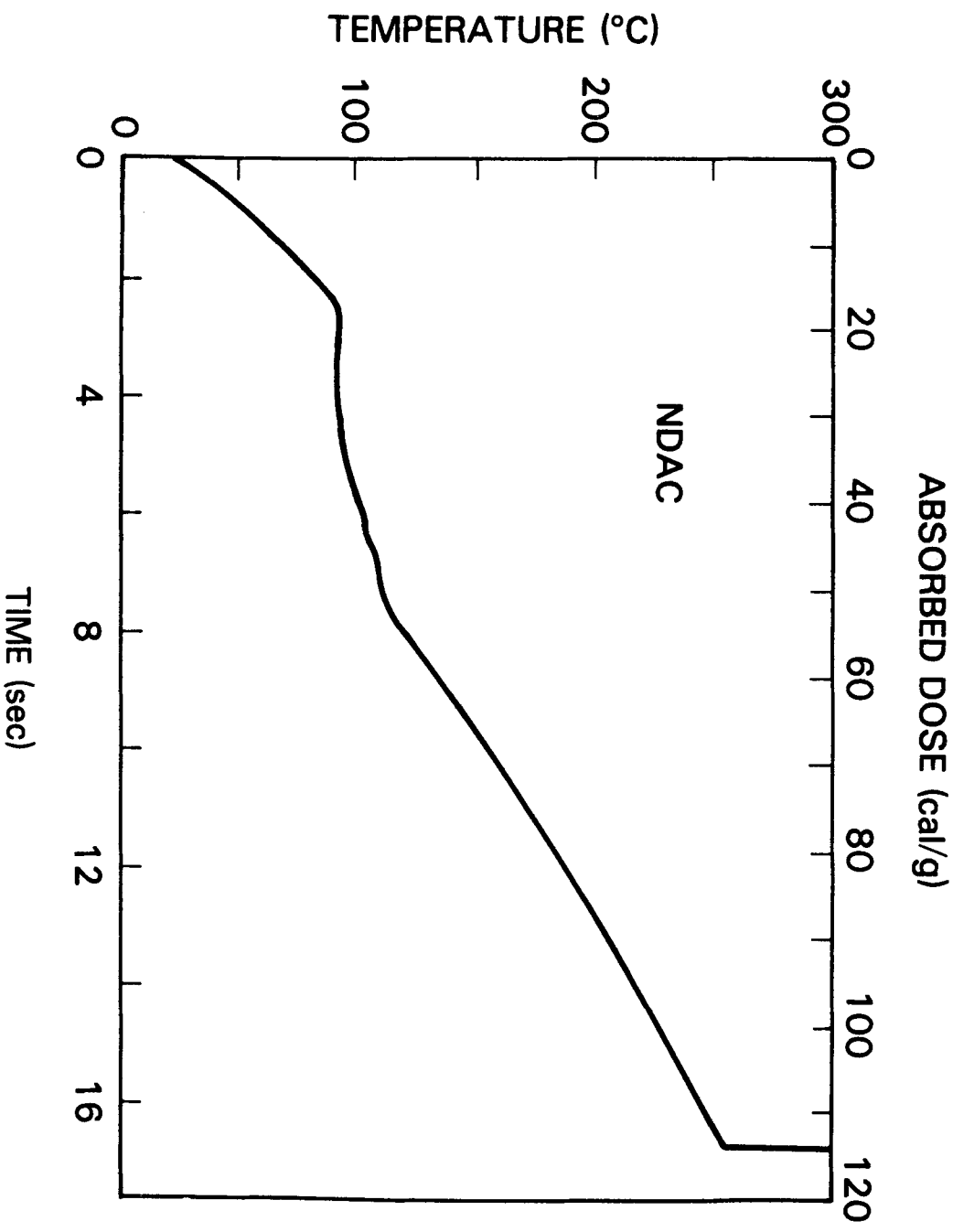

FIGURE 13
Thermal behavior of confined NDAC heated by beam.

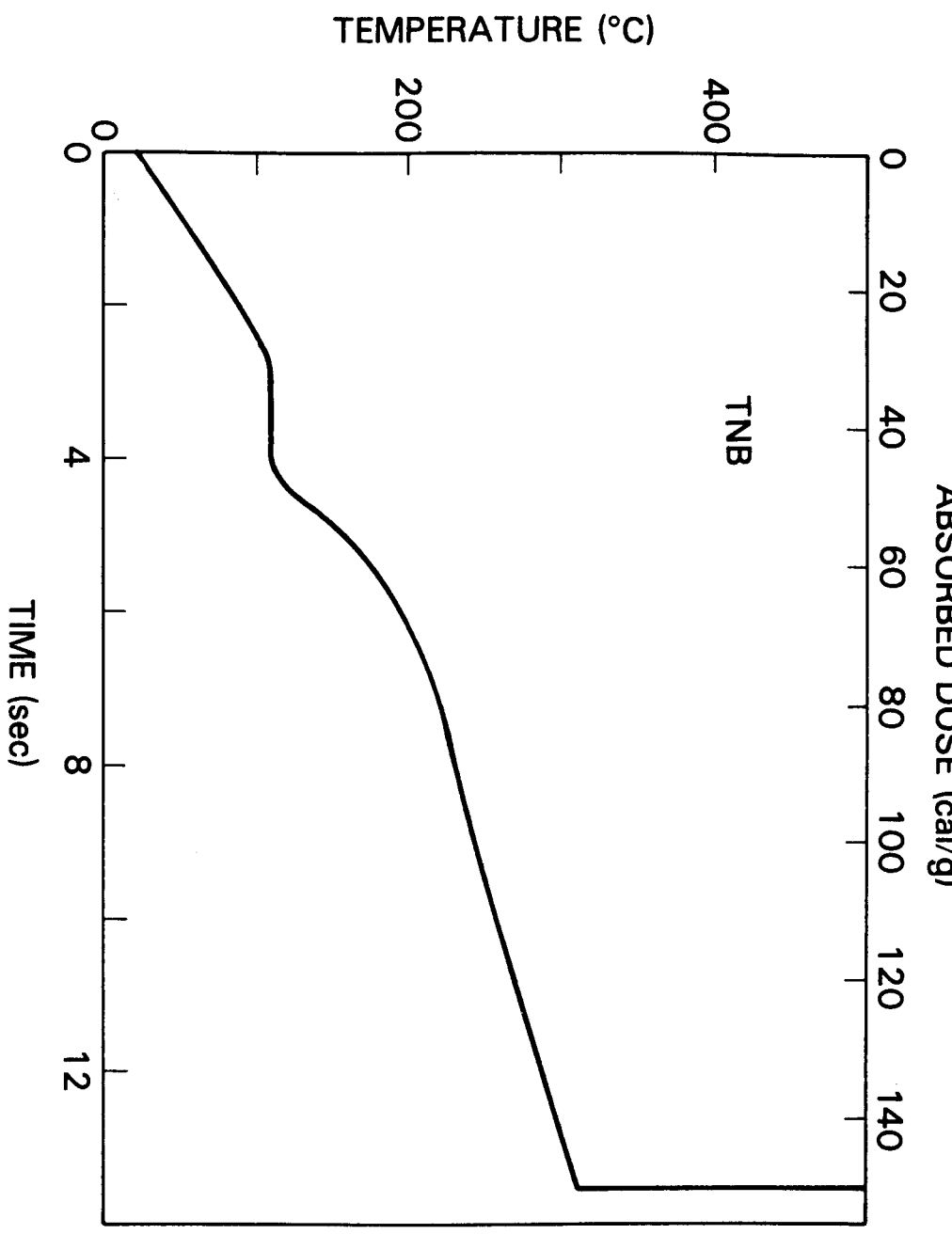

FIGURE 14
Thermal behavior of confined TNB under beam heating.

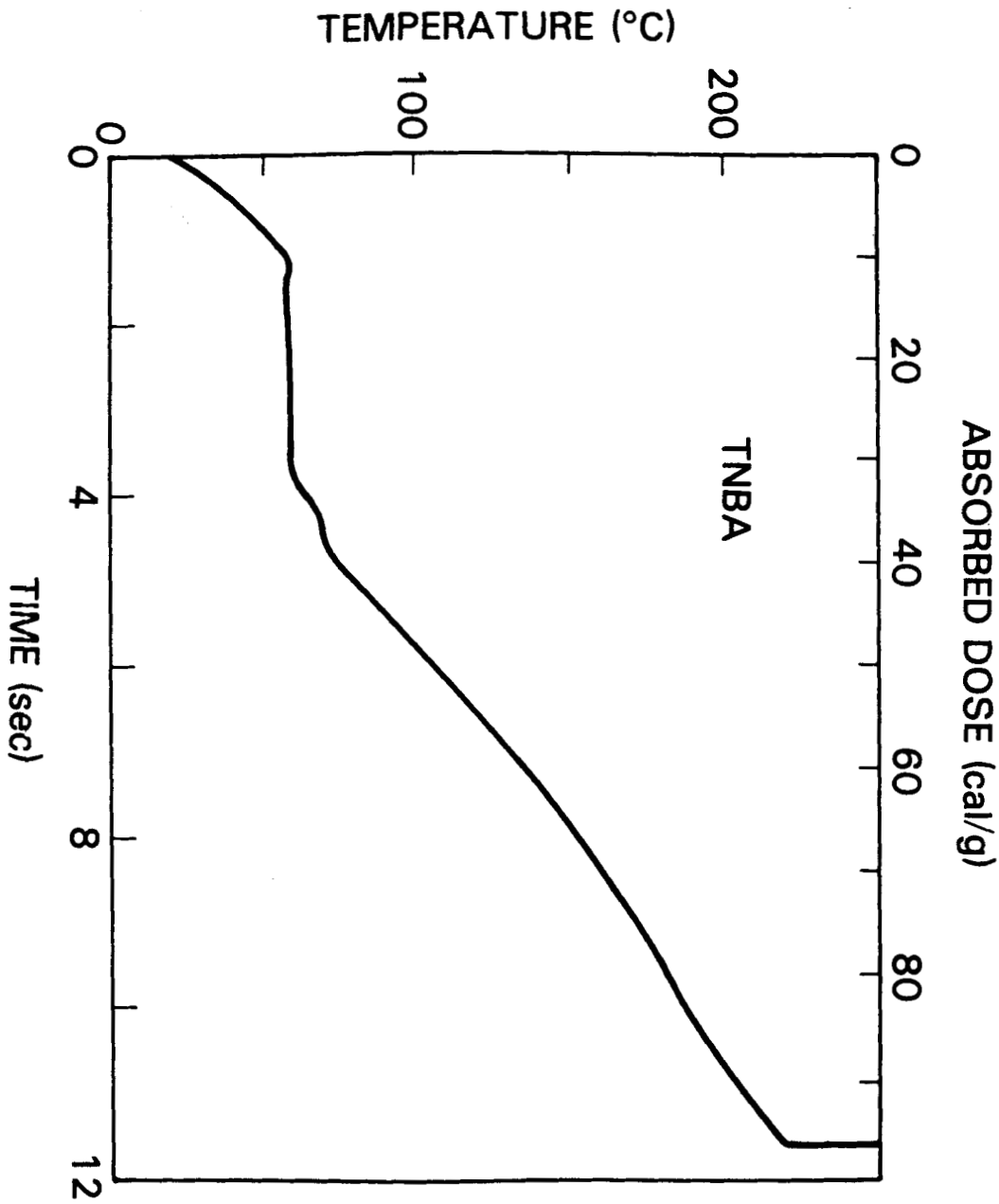

FIGURE 15
Thermal behavior of TNBA under beam heating.

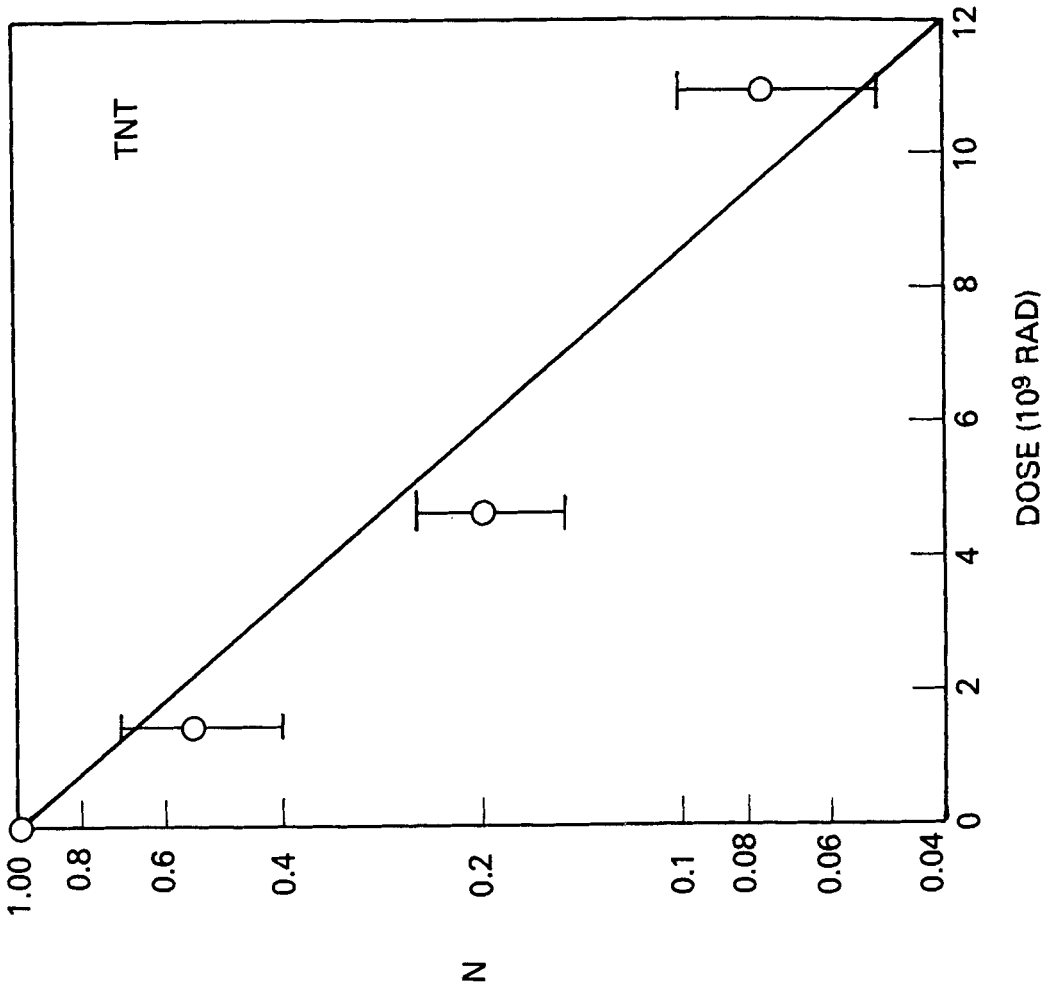

FIGURE 16
Fraction of original material for radiation-decomposed TNT vs total dose.

REFERENCES

1. See references and data in B.M. Dobratz and P.C. Crawford, LLNL Explosives Handbook, UCRL-52997 change 2, Jan. 1985.

2. D.L. Jaeger, Thermal Response of Spherical Explosive Charges Subjected to External Heating, LASL Report LA-8332, UC-45, Aug. 1980.

3. E. Catalano, R. McGuire, E. Lee, E. Wrenn, D. Ornellas, and J. Walton, Proceedings of the Sixth Symposium (International) on Detonation, Coronado, Ca., Aug. 1976, p. 214.

4. C.M. Tarver, R.R. McGuire, E.L. Lee, E. W. Wrenn, and K.R. Brein, Proceedings of the 17th International Combustion Symposium, Leeds, England, Aug. 1978, p. 1407.

5. R.R. McGuire and C.M. Tarver, Proceedings of the Seventh Symposium (International) on Detonation, Annapolis, Md., June 1981, p 56.

6. A.J. Th. Rooyers, M.W. Leeuw and A.C. van der Steen, Internationale Jahrestagung proceedings, Karlsruhe, Germany, 1982, p. 333, and private communication.

7. J. Wenograd, Trans. Farad. Soc. 57, 1612 (1961).

8. A.Stolovy, E.C. Jones, Jr., J.B. Aviles, Jr. and A.I. Namenson, Naval Research Laboratory Report 8350, Nov. 1979.

9. A. Stolovy, J.B. Aviles, Jr., E. C. Jones, Jr. and A.I. Namenson, Proceedings of the Seventh Symposium (International) on Detonation, Annapolis, Md., June 1981, p. 50.

10. A. Stolovy, E.C. Jones, Jr., J.B. Aviles, Jr., A.I. Namenson and W.A. Fraser, J. Chem. Phys. 78(1), 229 (1983).

11. P.V. Phung, J. Chem. Phys. 53(7), 2906 (1970).

12. T.R. Gibbs and A. Popolato, LASL Explosive Property Data, Univ of California Press, Berkeley, Ca., 1980, p. 233.

13. T.B. Brill and R.J. Karpowicz, J. Phys. Chem. 86, 4260 (1982).

14. J.M. Schnur, R.S. Miller, J.P. Sheridan and A.D. Britt, U.S. Patent No. 4097317 (June 27, 1978).

15. Samples prepared by A.D. Britt.

16. C.S. Coffey, private communication.

17. R. Petersen, Naval Weapons Station, Yorktown, VA. report TR 81-6 (Oct. 1981), and Explosives Hazard Index chart (1983).

18. M.G. Kendall and A. Stuart, The Advanced Theory of Statistics, Vol. 2, 3rd Edition, p. 496. Griffen, London (1973).

19. J. Sharma, private communication.

20. We are indebted to H.G. Adolph at NSWC for providing the samples and performing the chemical analysis.

21. S.P. Ahlen, Rev. Mod. Phys. 52, 121 (1980), P. 140.

22. J. Sharma, J.C. Hoffsommer, D.J. Glover, C.S. Coffey, F. Santiago, A. Stolovy and S. Yasuda, Proc. of APS Topical Conference on Shock Waves in Condensed Matter, Santa Fe, NM, July 18-21, 1983, P. 543.

23. D. Holtkamp, private communication.